Available online at www.sciencedirect.com
SCIENCE DIRECT
Journal of Molecular Catalysis A: Chemical 253 (2006) 176–186
JOURNAL OF MOLECULAR CATALYSIS A: CHEMICAL
www.elsevier.com/locate/molcata

Retention of the octahedral metal framework of Nb and Mo halide clusters in catalytic decomposition of phenyl acetate to phenol and ketene

Satoshi Kamiguchi [a], Takashi Mori [b], Masaki Watanabe [b], Akane Suzuki [c,d], Mitsuo Kodomari [b], Masaharu Nomura [c], Yasuhiro Iwasawa [d], Teiji Chihara [a,*]

[a] *The Institute of Physical and Chemical Research (RIKEN), Wako, Saitama 351-0198, Japan*
[b] *Department of Applied Chemistry, Shibaura Institute of Technology, Shibaura, Minato-ku, Tokyo 108-8548, Japan*
[c] *Photon Factory, Institute of Materials Structure Science, KEK, Ibaraki 305-0801, Japan*
[d] *Department of Chemistry, Graduate School of Science, the University of Tokyo, Hongo, Bunkyo-ku, Tokyo 113-0033, Japan*

Received 11 October 2005; received in revised form 13 March 2006; accepted 16 March 2006
Available online 2 May 2006

Abstract

When molecular chloride clusters of Nb, Mo, Ta, and W ($[(M_6Cl_{12})Cl_2(H_2O)_4]\cdot 4H_2O$ (M = Nb, Ta) and $(H_3O)_2[(M_6Cl_8)Cl_6]\cdot 6H_2O$ (M = Mo, W)) possessing an octahedral metal framework were treated in a helium stream above 200 °C, catalytic activity for the selective decomposition of phenyl acetate to phenol and ketene arose. The Fries rearrangement did not occur. The activity was ascribed to the Brønsted acidity of the hydroxo ligand that was formed by elimination of hydrogen chloride from the chloro and aqua ligands, and the selectivity was attributable to the large counter cluster anion that did not stabilize the intermediate protonated phenyl acetate and acetyl cations. The maximum activities of the Nb and Mo clusters appeared by activation at 250 °C and 400 °C, respectively, at which temperatures the retention of the octahedral cluster framework was ascertained by XDR analyses, Raman spectrometry, EXAFS spectrometry, and elemental analyses.
© 2006 Elsevier B.V. All rights reserved.

Keywords: Retention of cluster framework; Niobium halide cluster; Molybdenum chloride cluster; Decomposition of phenyl acetate; EXAFS

1. Introduction

Extensive efforts have been directed at the syntheses of halide clusters [1–4], and now 18 kinds of group 3–7 transition metal atoms combined with four kinds of π-donor halogen ligands are known to form halide clusters. However, studies on the reactivity of halide clusters have been quite limited. Reactivity with organic or inorganic reagents has been seen mainly in the field of ligand exchange reactions, an exception being a simple reaction with hydrogen that has been reported [5,6]. In contrast to carbonyl clusters, halide clusters have not been used as catalysts as far as we know [7–9], since the first typical halide cluster $MoCl_2$ was synthesized in 1859 [10]. Later, the formula of this cluster proved to be Mo_6Cl_{12} or more exactly $[Mo_6Cl_8^i]Cl_2^aCl_{4/2}^{a-a}$ (**1**) [11,12], where "*i*" and "*a*" refer to the inner and outer (außer) coordination spheres, respectively, and "*a*–*a*" refers to the corresponding linkage between two clusters [13]. Halide clusters are generally synthesized by comproportionation of metal powder with the corresponding mononuclear metal halide at above 650 °C. Such a treatment may make the halide clusters too stable to react with organic compounds and thus prevent their utilization as catalysts. Most of the halide clusters have an octahedral metal array structure with terminally coordinating, bridging, or triply bridging halogen π-donor ligands, constituting a multimetal multielectron system. The formal oxidation numbers of the metal atoms range from +1 to +3, which are intermediate between those of the bulk metal and the metal oxide. If some of the halogen ligands are removed or replaced with another ligand while leaving the metal framework intact, the exposed metal or the replaced ligand coordinated to metal atoms of an unusual oxidation state would react with organic substances in a unique fashion. In general, both the melting and boiling points of the clusters are quite high: for example, the melting point and the boiling point of **1** are estimated to be 1000 K and 1700 K, respectively [14]. The vapor pressure of **1** is accordingly quite low: the calculated vapor pressure of **1**

* Corresponding author. Tel.: +81 48 467 9399; fax: +81 48 462 4631.
E-mail address: chihara@riken.jp (T. Chihara).

1381-1169/$ – see front matter © 2006 Elsevier B.V. All rights reserved.
doi:10.1016/j.molcata.2006.03.038

at 237 °C is 10^{-6} atm [14], and the vapor pressure of $MoCl_4$, which is in equilibrium with **1**, over **1** has measured ~0.4 atm at 860 °C [15]. Hence, the metal framework is also stable at high temperatures. These thermodynamic stabilities are favorable for commercial use, if the halide clusters are employed as catalysts. Hence, attempts have been made to utilize the halide clusters as catalysts.

We have reported several reactions catalyzed by halide clusters. Two types have now been established for halide cluster catalysis: solid-acid catalysis and platinum-like catalysis. A variable selectivity, namely hydrogenolysis of the ethyl group of ethylbenzene under hydrogen and dehydrogenation under helium, is ascribable to the latter type [16]. Hydrogenation of cyclohexenone, hydrodehydration of cyclohexanone, and dehydrogenation of cyclohexene are also attributable to the latter type [17]. Dehydration of alcohols [18], isomerization of olefins [19], dehydrohalogenation of halogenated alkanes [20], isomerization of diethylbenzenes [21], methylation of toluene with methanol [22], and dehydrogenation of aliphatic amines [23] are assigned to the former type.

Aromatic acylation is an important process in the fine chemical industries and has been intensively investigated. The reaction of phenyl acetate to *o*- and *p*-hydroxyacetophenone is well known as the Fries rearrangement [24], and usually Lewis acids such as $AlCl_3$, BF_3, $FeCl_3$, and $TiCl_4$ are used stoichiometrically. Because the carbonyl oxygen strongly coordinates to the Lewis acid center [25], hydrolysis of the Lewis acid is necessary for the isolation of the products. In order to overcome this disadvantage, solid Brønsted acids such as H-Beta zeolite [26–29], H-Y zeolite [28,30,31], H-ZSM-5 [26–28,30–33], HF/Al_2O_3 [30], and Nafion-H [34], a resin containing the $–CF_2CF_2SO_3H$ group, are used as the catalyst. However, the selectivity for *o*- and *p*-hydroxyacetophenone is not high, and in almost all cases the main product is the decomposition product, phenol. For example, when the various solid acids were used in cumene at 150 °C, phenol was obtained in 41–66% selectivity with *o*- and *p*-hydroxyacetophenone in 19–57% selectivity [34]. In order to obtain *o*- and *p*-hydroxyacetophenone efficiently phenol was used as the solvent, and the selectivity was seemingly enhanced to 57–95% [34]. In this reaction, the produced ketene was captured by the solvent, phenol. Thus, the decomposition to phenol and ketene is inevitable. Application of the halide cluster catalyst to the Fries rearrangement was unsuccessful; however, decomposition of phenyl acetate to phenol and ketene unexpectedly proceeded exclusively at as low as 150 °C. Pyrolysis of phenyl acetate requires heating above ca. 700 °C [35,36], and no other catalysts for the selective decomposition at lower temperature have been reported. We have reported the reaction in a preliminary paper [37]. In order to understand the nature of the cluster catalyst as well as to shed light on the mechanism of the Fries rearrangement over a solid acid catalyst and accordingly to design improved catalysts, a detailed investigation has been performed. We report here the results, and the activation mechanism of the halide clusters and the retention of the cluster framework are also shown.

2. Experimental

2.1. Materials and catalytic measurement

The cluster complexes $[(Nb_6Cl^i_{12})Cl^a_2(H_2O)_4]\cdot 4H_2O$ (**2**) [38], $[(Nb_6Br^i_{12})Br^a_2(H_2O)_4]\cdot 4H_2O$ [38], $(H_3O)_2[(Mo_6Cl^i_8)Cl^a_6]\cdot 6H_2O$ (**3**) [39], $[Mo_6Cl^i_8]Cl^a_2Cl^{a-a}_{4/2}$ (Mo_6Cl_{12}, **1**) [39], $[(Ta_6Cl^i_{12})Cl^a_2(H_2O)_4]\cdot 4H_2O$ [38], and $(H_3O)_2[(W_6Cl^i_8)Cl^a_6]\cdot 6H_2O$ [40] were prepared according to the published procedures. The cluster $Re_3Cl_9([Re_3Cl^i_3]Cl^a_3Cl^{a-a}_{6/2})$ was commercially available. The crystals of these complexes were crushed and screened to 150–200 mesh.

A conventional vertical glass fixed-bed microreactor with a continuous flow system was operated at atmospheric pressure [19]. Typically, a weighed cluster sample (30 mg) was packed in a borosilicate glass tube (3 mm i.d.). The catalyst sample was initially treated in situ at a fixed temperature (r.t. −500 °C) for 1 h in a helium stream (2.4 L/h). The reaction was then started by feeding phenyl acetate (0.10 mL/h, 0.79 mmol/h) into the stream of helium at the treatment temperature or 150 °C. The reaction was monitored by sampling the reaction gas (0.3 mL) followed by analyses using an online GLC.

2.2. Characterization

Reaction products were analyzed by an online GLC (Shimadzu 14B) equipped with an FID detector using a polyethylene glycol 20,000 column. The formation of phenol was identified by comparison with an authentic sample. The formation of ketene was confirmed by bubbling the reaction gas to ethanol and isopropyl alcohol traps to produce ethyl acetate and isopropyl acetate, respectively. Analyses of the trapped and gaseous products revealed the formation of phenol and ketene almost exclusively. A trace amount of benzene was detected, but its selectivity was less than 0.5% under helium.

Raman spectra of the cluster samples in the reaction glass tubes employed were recorded in situ on a Kaiser Optical Systems HoloLab 5000 with an Nd-YAG laser operated at 532 nm and with a 7.6-mm focus lens. The data counts were accumulated 30 times at 1-s intervals. Then powder X-ray diffraction (XRD) analysis was performed on 20-mg samples using a Rigaku RAD-3R X-ray diffractometer employing Cu Kα radiation at a scan rate of $2^\circ\ min^{-1}$. Diffuse reflectance FT-IR spectra of the cluster samples were recorded on a Shimadzu IRPrestige-21, and ATR-FTIR spectra of the cluster samples were recorded on a SensIR Technologies TravelIR with a ZnSe beam splitter.

EXAFS spectra at the Nb and Mo K edges were recorded in transmission mode at BL-10B of KEK-PF using an Si(311) channel-cut crystal monochromator and ionization chambers, and were analyzed using the UWXAFS program [41]. After background subtraction by the AUTOBK program [42], Fourier transformation for the k^3-weighted EXAFS oscillation was performed, and the structural parameters were determined by a curve fitting procedure in *R*-space by using the FEFFIT program involving multiple scattering effects

(Eq. (1)) [43]:

$$\chi(k) = \sum_j S_0^2 N_j \frac{F_j(k)}{kR_j{}^2} \sin(2R_j k + \delta_j(k)) \times \exp\left(-2k^2\sigma_j{}^2 - \frac{2R_j}{\lambda_j(k)}\right), \quad (1)$$

where $F_j(k)$ is the backscattering amplitude from each of the N_j scatterers at distance R_j from the X-ray absorbing atom, $\delta_j(k)$ the central-atom phase shift, σ_j^2 the mean square fluctuation in R_j, $\lambda_j(k)$ the mean free path of the photoelectron, and S_0^2 the overall amplitude reduction factor. The values of $F_j(k)$, $\delta_j(k)$, and $\lambda_j(k)$ were generated by the FEFF code. The high-precision static EXAFS data were analyzed in the range of $0.08 \leq R/\text{nm} \leq 0.60$ by considering all the single- and multiple-scattering contributions.

3. Results and discussion

3.1. Development of catalytic activity

Undiluted crystal powder of the halide cluster $[(Nb_6Cl_{12})Cl_2(H_2O)_4]\cdot 4H_2O$ (**2**) in a glass reaction tube was initially treated in a helium stream for 1 h at an elevated temperature, and then reaction was commenced by introducing phenyl acetate into the gas flow without changing the temperature. The reaction profiles at various temperatures are plotted in Fig. 1. No catalytic activity was observed below 100 °C, and slight activity was evident at 150 °C. Treatment above 200 °C resulted in substantial catalytic activity for **2** and the activity increased with increasing temperature, reaching a maximum at 300 °C. Thermal treatment of the cluster gave rise to catalytic activity. The products were solely phenol and ketene, and no by-products such as *o*- and *p*-hydroxyacetophenone were detected throughout the reactions.

As can be seen from Fig. 1, the catalytic activity versus time decreased very rapidly during the first 2 h of the reaction and leveled off after 3 h of the reaction. This is probably due to a deposit of coke on the catalyst [31,33]. Rapid deactivation of zeolitic catalysts particularly in the gas phase reaction owing to coke formation has been reported in the initial stage of this reaction [27]. The deactivation was increased by an increase in the reaction temperature; a similar temperature effect is also reported on H-ZSM-5 for this reaction [26]. The catalytic activity will henceforth be discussed at 3 h after reaction started. The conversion was proportional to the amount of cluster **2**. The reaction rate was almost proportional to the amount of phenyl acetate added up to 0.025 mL/h. At higher feeding above 0.05 mL/h the reaction showed zero-order kinetics, indicating the saturated adsorption of phenyl acetate, and subsequent experiments were performed in this region.

The catalytic activities of various halide clusters and the related compound tested are listed in Table 1. This Table shows that Nb metal had no catalytic activity. Niobium pentachloride could not be applied to the catalysis under the same reaction conditions, as it begins to sublime at 125 °C. These results clearly show that **2** developed into a novel catalyst at a high temperature by taking advantage of its low vapor pressure and high melting point. Halide clusters would be promising solid catalysts as metal halides that can be used at elevated temperatures. Table 1 also shows that a bromide cluster of Nb and chloride clusters of Mo, Ta, and W also exhibited similar catalytic activities. Under a hydrogen stream, clusters **2** and **3** catalyzed the decomposition of phenyl acetate similarly. However, hydrogenolysis to benzene proceeded in around 20% selectivity, which could be attributable to the platinum-like property of the cluster catalysts [16,17].

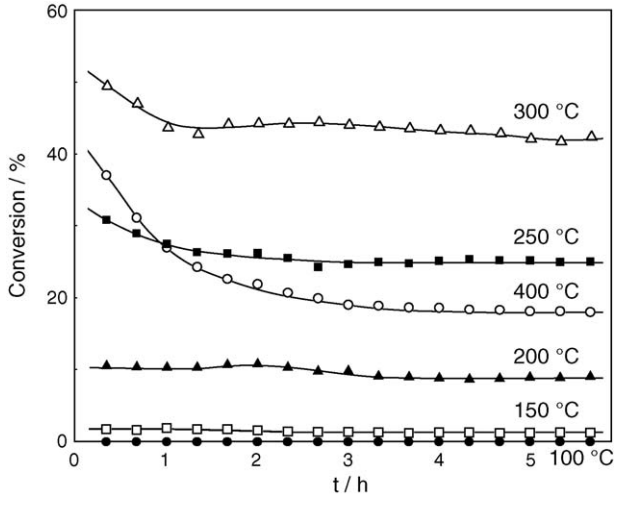

Fig. 1. Reaction profile of phenyl acetate catalyzed by $[(Nb_6Cl_{12})Cl_2(H_2O)_4]\cdot 4H_2O$ (**2**) at different temperatures. After treatment of **2** (30 mg) in a helium stream (2.4 L/h) for 1 h, reaction was initiated by introduction of phenyl acetate (0.1 mL/h) to the helium stream at the treatment temperature. Decomposition to phenol and ketene proceeded exclusively. Conversion = phenol/(phenyl acetate + phenol) × 100 (%).

Table 1
Catalytic activity of halide clusters for decomposition of phenyl acetate to phenol and ketene[a]

Catalyst	Conversion (%)[b]
$[(Nb_6Cl_{12})Cl_2(H_2O)_4]\cdot 4H_2O$ (**2**)	25.3
$[(Nb_6Cl_{12})Cl_2(H_2O)_4]\cdot 4H_2O$ (**2**)	67.1[c]
$[(Nb_6Br_{12})Br_2(H_2O)_4]\cdot 4H_2O$	48.9
$(H_3O)_2[(Mo_6Cl_8)Cl_6]\cdot 6H_2O$ (**3**)	5.6
$(H_3O)_2[(Mo_6Cl_8)Cl_6]\cdot 6H_2O$ (**3**)	82.6[d]
$[(Ta_6Cl_{12})Cl_2(H_2O)_4]\cdot 4H_2O$	3.2
$(H_3O)_2[(W_6Cl_8)Cl_6]\cdot 6H_2O$	6.2
Re_3Cl_9	0.5
Nb metal	0.0
None	0.0

[a] Catalysts were treated at 250 °C for 1 h followed by reaction at the same temperature. Only phenol and ketene were formed under a helium stream. Catalyst: 30 mg (150–200 mesh), helium: 2.4 L/h, phenyl acetate: 0.1 mL/h (0.79 mmol/h).

[b] Conversion = aromatic compounds/(aromatic compounds + phenyl acetate) × 100 (%) after 3 h of reaction.

[c] Under a hydrogen stream (2.4 L/h). Phenol (78.8%), benzene (16.5%), toluene (2.8%), and naphthalene (1.9%) were produced with ketene.

[d] Under a hydrogen stream (2.4 L/h). Phenol (68.3%), benzene (25.5%), toluene (3.7%), and naphthalene (2.5%) were produced with ketene.

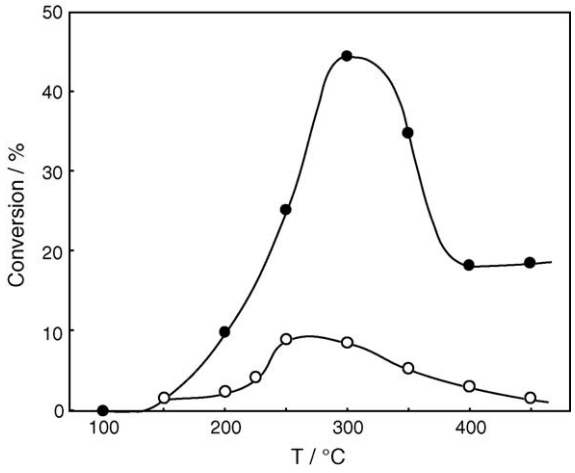

Fig. 2. Effect of preliminary treatment temperature and reaction temperature on catalytic activity of $[(Nb_6Cl_{12})Cl_2(H_2O)_4]\cdot 4H_2O$ (**2**). After treatment of **2** (30 mg) in a helium stream (2.4 L/h) at a different temperature for 1 h, reaction was initiated by introduction of phenyl acetate (0.1 mL/h) to the helium stream at the treatment temperature (●) or at 150 °C (◯). Conversion = phenol/(phenyl acetate + phenol) × 100 (%) at 3 h.

3.2. Activation of $[(Nb_6Cl_{12})Cl_2(H_2O)_4]\cdot 4H_2O$ (2)

The effect of the preliminary treatment temperature on $[(Nb_6Cl^i_{12})Cl^a_2(H_2O)_4]\cdot 4H_2O$ (**2**) and successive reaction temperature was examined, and the results are summarized in Fig. 2. When both temperatures were changed concomitantly, the maximum activity appeared at 300 °C. On the other hand, when the subsequent reactions were performed at 150 °C, the maximum activity appeared at around 250 °C. Hence, preliminary treatment at 250 °C induced the highest catalytic activity for **2**.

The X-ray diffraction patterns of **2** treated at various temperatures for 1 h are depicted in Fig. 3. The change of the pattern shows that treatment above 100 °C changed **2** to an amorphous compound that is not the extended Nb–Cl–Nb bonded binary solid-state cluster $Nb_6Cl_{14}([Nb_6Cl^i_{10}Cl^{i-a}_{2/2}]Cl^{a-a}_{4/2}Cl^{a-i}_{2/2})$, which is prepared by direct reaction of Nb metal with $NbCl_5$ [44]. Furthermore, the change of the crystal structure at 100 °C, which would be caused by removal of the crystal water [45], did not give rise to catalytic activity.

The Raman spectra of the treated samples are shown in Fig. 4. The spectra markedly changed at 250 °C with increasing temperature. The Raman shift caused by the vibration of Nb–Cl^a or Nb–O^a has not been attributed for this complex. However, the band at 239 cm^{-1} is assigned to the breathing motion of the Nb_6 octahedron (A_{1g}), and those at 161 and 152 cm^{-1} are attributed to edge bridging Nb–Cl^i breathing vibrations (E_g and T_{2g}, respectively) [46]. Crystal structural data revealed that the differences in M–M distances parallel the observed variations in the Raman shift [47]. The variations in the observed shift of the M_6 A_{1g} band are almost entirely accounted for by differences in the M–M force constant that accompany changes in the M–M bond distances [47]. The band of the Nb_6 A_{1g} vibration mode begins to shift to higher energy by treatment and has a maximum shift at 250 °C. The loss of some internal Cl ligands can increase the Nb–Nb bond order of the Nb_6 octahedron, which may be ascribed to the higher energy shift [47]. Nevertheless, the Nb_6 metal framework remains intact. Above 250 °C the two Raman bands originally at 161 and 152 cm^{-1} due to edge bridging Nb–Cl^i breathing vibrations are replaced with a new band, which suggests that the coordination mode of the inner Cl ligands changed above this temperature. At this temperature the catalytic activity was the highest. Hence, the catalytic activity of **2** can be attributed to the loss of the inner Cl ligands with retention of the cluster framework. Evolution of HCl was observed when **2** was treated above 150 °C. Loss of the Cl atom is evident and the origin of the H atom in HCl can be aqua ligand. No appreciable changes of the Raman spectra were observed after 3 h catalytic reaction at 150 °C. Even though Raman peaks attributable to the organic material appear after reaction, the peaks appear generally in the higher wavenumber region, as the organic material comprises light atoms.

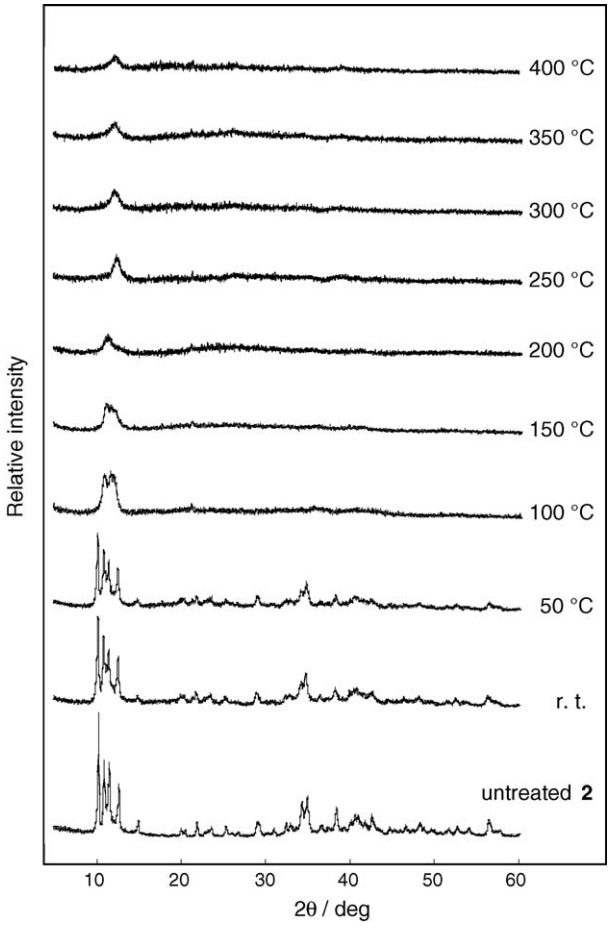

Fig. 3. XRD patterns of $[(Nb_6Cl_{12})Cl_2(H_2O)_4]\cdot 4H_2O$ (**2**) treated at various temperatures in a helium stream for 1 h.

The diffuse reflectance FT-IR spectra of **2** and the 250 °C-treated sample were measured. A sharp band at 397 cm^{-1} appeared after this treatment. A Nb–OH bond of a hydroxo ligand was formed by this treatment as exemplified in Eq. (2), since a Nb–OH_2 bond of an aqua ligand has no peaks in this region [48].

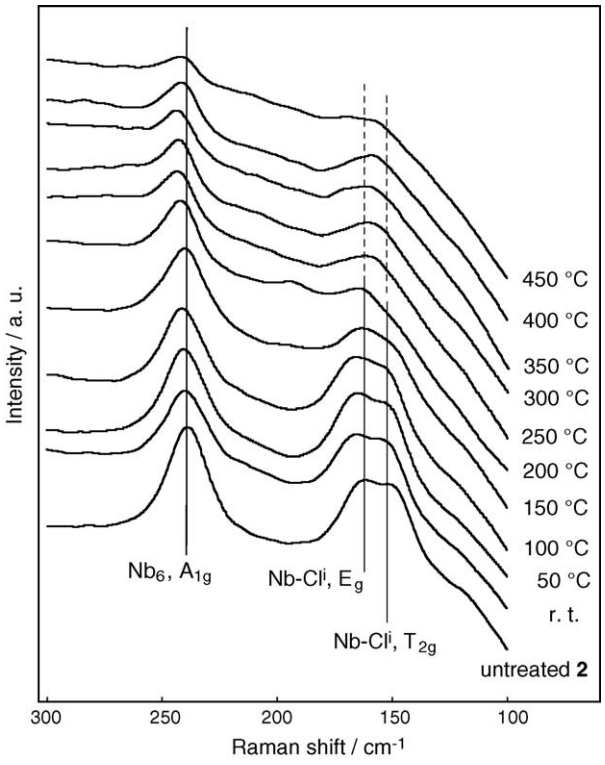

Fig. 4. Raman spectra of $[(Nb_6Cl_{12})Cl_2(H_2O)_4]\cdot 4H_2O$ (**2**) treated at various temperatures in a helium stream for 1 h.

$$[(Nb_6Cl_{12})Cl_2(H_2O)_4]\cdot 4H_2O(\mathbf{2}) \rightarrow [(Nb_6Cl_{12})Cl(H_2O)_3(OH)] + 4H_2O + HCl \quad (2)$$

The IR spectrum of crystalline **2** treated at 250 °C in a helium stream followed by adsorption of pyridine is illustrated in Fig. 5 with related spectra. A band at around 1601 cm^{-1} attributable to the cluster is common in each spectrum. The band at 1441 cm^{-1} was assigned to hydrogen bonded pyridine [49,50], as untreated **2** has crystal water and aqua ligand. Three bands at 1634, 1536, and 1486 cm^{-1} assignable to pyridinium ion in the spectrum of **2** treated at 250 °C show the presence of a Brønsted acid site on **2** [49,51]. However, there is no band that is characteristic of coordinatively bonded pyridine in the 1447–1460 cm^{-1} region [49], and hence there is no Lewis acid site.

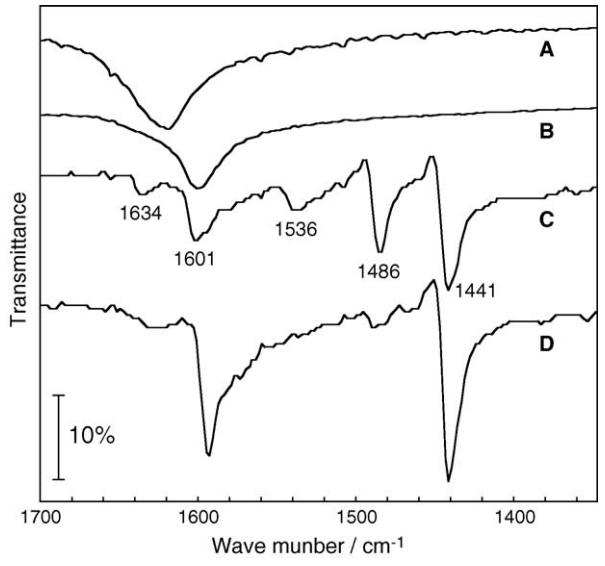

Fig. 5. IR spectra of pyridine adsorbed on $[(Nb_6Cl_{12})Cl_2(H_2O)_4]\cdot 4H_2O$ (**2**). Crystals of **2** (A) were treated in a helium stream at 250 °C for 1 h (B), followed by introduction of pyridine (C). Pyridine was introduced to the crystals of **2** without thermal activation (D).

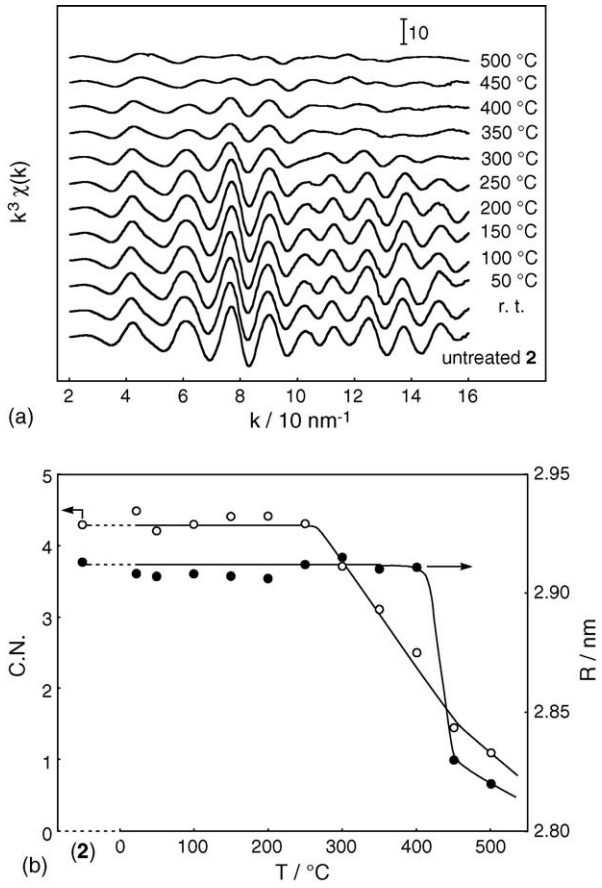

Fig. 6. (a) The k^3-weighted EXAFS oscillations at the Nb K-edge for $[(Nb_6Cl_{12})Cl_2(H_2O)_4]\cdot 4H_2O$ (**2**) treated at various temperatures in a helium stream for 1 h, and (b) values of coordination number (C.N., ◯) and bond length (R, ●) determined by curve fitting.

The EXAFS spectra of the near Nb K-edge absorption region for the treated samples, and the value of the coordination number (C.N.) of Nb–Nb and the bond length determined by curve fitting are plotted in Fig. 6. The Nb–Nb bond length of 0.291 nm, which corresponds to the Nb_6 octahedron, was maintained up to 400 °C and the values of C.N. for Nb–Nb were retained up to 250 °C with increasing treatment temperature. Accordingly, the most active species that was formed by 250 °C treatment retained the octahedral cluster framework. In addition, the cluster framework obviously disintegrated above 450 °C, indicating the catalytic inertness of the metal fragments. In the case of carbonyl clusters that contain group 8–10 transition metals, metal–metal bond is weaker than metal–CO bond and metal fragments formed by decomposition of the clusters can be the catalytically active species. No appreciable changes in the EXAFS spectra were observed after subsequent 3 h reaction at 150 °C.

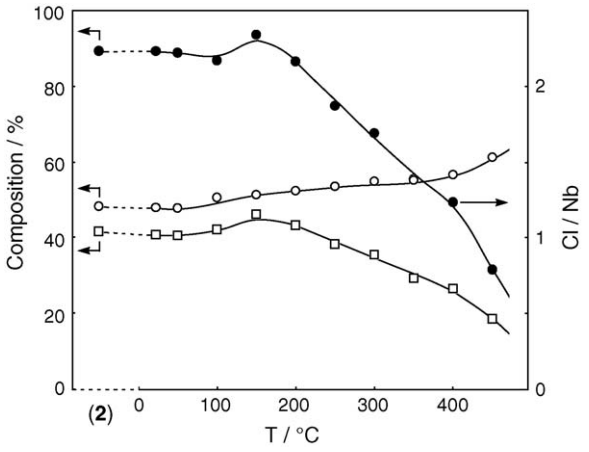

Fig. 7. Analytical data for $[(Nb_6Cl_{12})Cl_2(H_2O)_4]\cdot 4H_2O$ (**2**) treated at various temperatures in a helium stream (2.4 L/h) for 1 h. Analytical data for intact **2** are also plotted. Nb (◯), Cl (□), and the atomic number ratio of Cl/Nb (●).

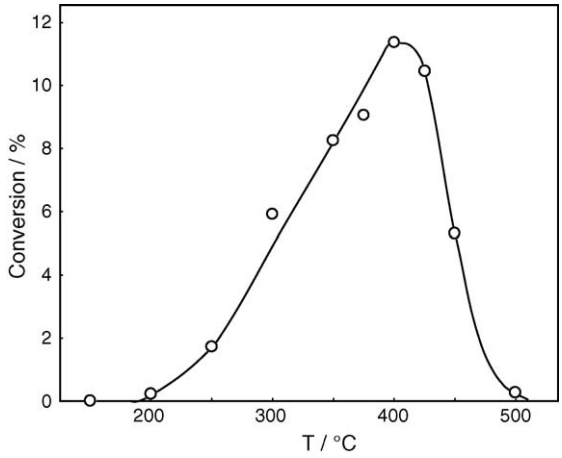

Fig. 8. Effect of preliminary treatment temperature on catalytic activity of $(H_3O)_2[(Mo_6Cl_8)Cl_6]\cdot 6H_2O$ (**3**). After treatment of **3** (30 mg) in a helium stream (2.4 L/h) at a different temperature for 1 h, reaction was initiated by introduction of phenyl acetate (0.1 mL/h) to the helium stream at 150 °C. Conversion = phenol/(phenyl acetate + phenol) × 100 (%) at 3 h.

The analytical data of Nb and Cl atoms in the treated samples are depicted in Fig. 7. The Cl content of **2** and consequently the relative amount of Cl to Nb decreased definitely above 200 °C with an increase in the treatment temperature. Experimentally, $Nb_6Cl_{11.2}$ species on average were formed by treatment at 250 °C, which correspond to the most catalytically active species. Since outer halogen ligands are generally labile and hence are replaced prior to the inner ligands [39], loss of the inner Cl ligands commenced at this stage, which is consistent with the results obtained by Raman and IR analyses. Above this temperature substantial loss of the Cl ligand and decrease of the catalytic activity started with increasing treatment temperature.

Thus, when cluster **2** was treated progressively with increasing temperature in a helium stream, its crystal structure decayed at 100 °C by losing the crystal water, loss of the Cl ligand commenced at 200 °C, and loss of the inner Cl ligand was evident at 250 °C with retention of the Nb_6 cluster framework, at which temperature the maximum catalytic activity appeared. Above 250 °C the significant elimination of the Cl ligand led to partial decomposition of the molecular cluster, and above 450 °C the Nb_6 octahedron practically decayed. The fragments of the broken cluster exhibited no catalytic activity.

3.3. Activation of $(H_3O)_2[(Mo_6Cl_8)Cl_6]\cdot 6H_2O$ (3)

Fig. 8 shows the catalytic activity of $(H_3O)_2[(Mo_6Cl_8^i)Cl_6^a]\cdot 6H_2O$ (**3**), which underwent preliminary treatment at various temperatures in a helium stream for 1 h and was then reacted at 150 °C. The activity emerged with treatment above 200 °C and reached a maximum with treatment at 400 °C, then it waned with treatment at 500 °C.

The XRD patterns of **3** treated at various temperatures for 1 h in a helium stream are illustrated in Fig. 9. The cluster chemistry of molybdenum(II) chloride has been extensively investigated. The XRD pattern of **3** treated at ambient temperature matches exactly that of $[(Mo_6Cl_8)Cl_4(H_2O)_2]\cdot 6H_2O$ (**4**) [52]. In this reaction, two Cl ligands in **3** were removed as HCl yielding an aqua complex **4** (Eq. (3)).

$$(H_3O)_2[(Mo_6Cl_8)Cl_6]\cdot 6H_2O(\mathbf{3}) \xrightarrow{\text{r.t.}} [(Mo_6Cl_8)Cl_4(H_2O)_2]\cdot 6H_2O(\mathbf{4}) + 2HCl \quad (3)$$

The XRD pattern of **3** treated at 100–150 °C showed a transformation to another complex. The single-crystal X-ray structure determination of $[(Mo_6Br_8)Br_4(H_2O)_2]$ has been reported [53], and its chloride analogue, $[(Mo_6Cl_8)Cl_4(H_2O)_2]$ (**5**), is known to be its isomorph. However, only the lattice constants of the latter have been reported [54]. The XRD pattern of the 150 °C-treated sample accords with that of $[(Mo_6Br_8)Br_4(H_2O)_2]$, and the lattice constants of the treated sample agree with those reported for **5**. Elemental analyses of the 150 °C-treated sample for Mo (55.0%) and Cl (41.0%) also support the formation of **5**. Hence, **4** was transformed to **5** by elimination of the crystal water (Eq. (4)).

$$[(Mo_6Cl_8)Cl_4(H_2O)_2]\cdot 6H_2O(\mathbf{4}) \xrightarrow{150\,^\circ C} [(Mo_6Cl_8)Cl_4(H_2O)_2](\mathbf{5}) + 6H_2O \quad (4)$$

The XRD patterns of the samples treated above 250 °C reveal conversion into an extended Mo–Cl–Mo bonded solid-state cluster $[Mo_6Cl_8^i]Cl_2^aCl_{4/2}^{a-a}$ (**1**) (Eq. (5)) [11,12]. The half-band width of the peaks at 12.6° and 15.6° became narrower when the sample was heated from 250 °C to 400 °C, indicating an increasing crystallinity with increasing treatment temperature. There were no changes of the XRD patterns after 3 h reactions at 150 °C.

$$[(Mo_6Cl_8^i)Cl_4^a(H_2O)_2](\mathbf{5}) \xrightarrow{>250\,^\circ C} [Mo_6Cl_8^i]Cl_2^aCl_{4/2}^{a-a}(\mathbf{1}) + 2H_2O \quad (5)$$

The Raman spectra of the treated samples are shown in Fig. 10, in which some of the assigned peaks for the molecular cluster **3** are indicated [47,55]. The Raman spectra of halide clusters are generally insensitive to ligand exchange. For example, the

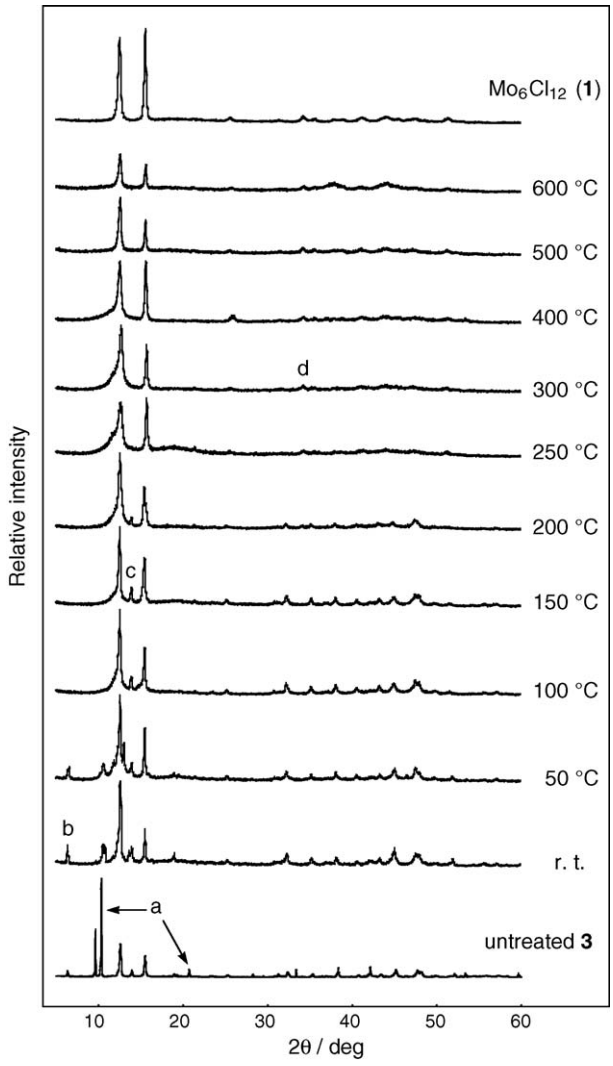

Fig. 9. XRD patterns of $(H_3O)_2[(Mo_6Cl_8)Cl_6]\cdot 6H_2O$ (**3**) treated at various temperatures in a helium stream for 1 h. The XRD pattern of authentic Mo_6Cl_{12} (**1**) is also shown. All the identified compounds have two strong diffraction peaks at 12.4–12.6° and 15.3–15.6°. Unique diffraction peaks of each compound are indicated: (a) for **3**, (b) for $[(Mo_6Cl_8)Cl_4(H_2O)_2]\cdot 6H_2O$ (**4**), (c) for $[(Mo_6Cl_8)Cl_4(H_2O)_2]$ (**5**), and (d) for **1**.

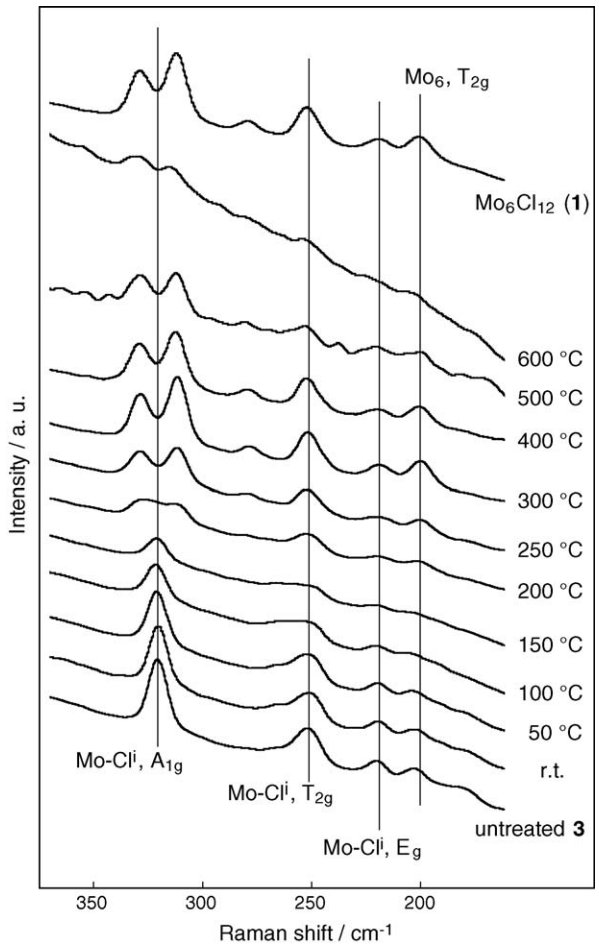

Fig. 10. Raman spectra of $(H_3O)_2[(Mo_6Cl_8)Cl_6]\cdot 6H_2O$ (**3**) treated at various temperatures in a helium stream for 1 h. The Raman spectrum of authentic Mo_6Cl_{12} (**1**) is also shown.

Raman spectrum of $(C_6H_5CH_2NMe_3)_2[(Mo_6Cl_8)Cl_6]$ is quite similar to that of $[(Mo_6Cl_8)Cl_4(THF)_2]$ [47]. This observation demonstrates that the change in outer ligands from Cl to an oxygen donor does not grossly affect the symmetry of the molecule. The spectra of **3** and the samples treated up to 150 °C are highly similar, which accords with the reactions expressed by Eqs. (3) and (4). On the other hand, the spectra of the 250–600 °C-treated samples are quite similar to that of authentic **1** [47,56]. Thus, the result from Raman spectrometry accords with the discussion on the XRD analyses. No appreciable changes of the Raman spectra were observed after subsequent 3 h reactions at 150 °C.

The EXAFS spectra of the near Mo K-edge absorption region for the treated samples, and the values of C.N. for Mo–Mo and the bond length determined by curve fitting are plotted in Fig. 11. There are only small changes in the EXAFS spectra for treatment up to 400 °C. The value of C.N. for Mo–Mo was unchanged up to 400 °C, this value corresponding to the Mo_6 octahedron. The Mo–Mo distance of the cluster framework was also retained up to 450 °C. These findings accord with the change of **3** via **4** and **5** to **1**, all of which have the same C.N. and Mo–Mo distance, and hence prove that the 400 °C-treated sample, which exhibited the maximum catalytic activity, retained the Mo_6 cluster framework. Treatment above 450 °C caused a significant decrease in both the C.N. and Mo–Mo distance. Decreasing intensity of the XRD peaks above 500 °C as shown in Fig. 9 is attributable to the partial decay of **1**. In contrast, it is speculated that complex **1** is stable up to 600 °C [57] and begins to disproportionate to gaseous $MoCl_4$ and Mo metal at about 730 °C in an inert atmosphere [58,59], although **1** decomposes above 430 °C under hydrogen [60]. There were no peaks assignable to Mo metal in the XRD patterns up to 600 °C. Aggregation of the metallic molybdenum would be prevented because of the high Tammann temperature, even if metallic molybdenum was formed. No appreciable changes in the EXAFS spectra were observed after subsequent 3 h reactions at 150 °C.

Fig. 12 shows analytical data of Mo and Cl atoms in the treated samples. The Mo fraction increased with increasing treatment temperature, because Mo is not volatile unless it changes to $MoCl_x$ ($x = 4$, 5) or $MoCl_2O_2$. Fig. 12 also shows that the ratio of Cl to Mo decreased with an increase in

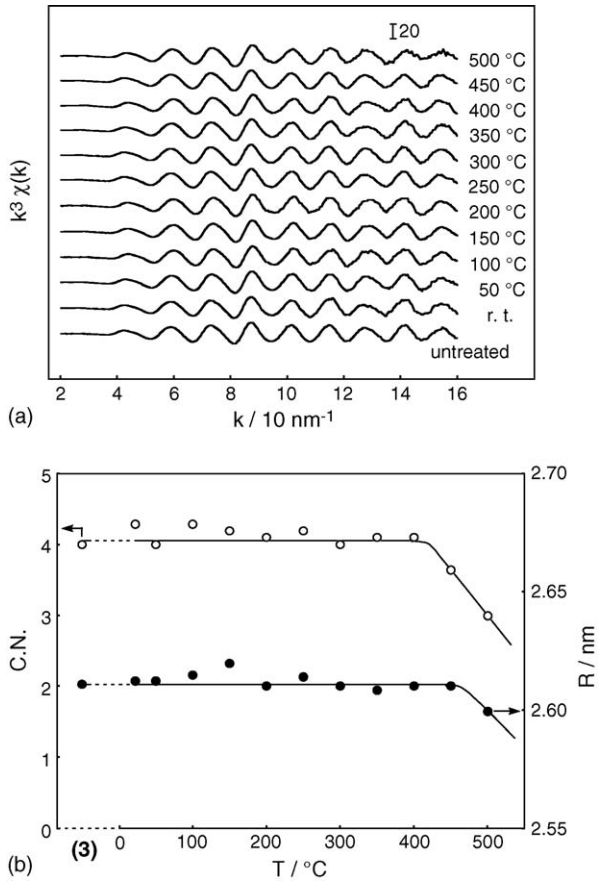

Fig. 11. (a) The k^3-weighted EXAFS oscillations at the Mo K-edge for $(H_3O)_2[(Mo_6Cl_8)Cl_6]\cdot 6H_2O$ (**3**) treated at various temperatures in a helium stream for 1 h, and (b) values of coordination number (C.N., ◯) and bond length (R, ●) determined by curve fitting.

treatment temperature. Although the 400 °C-treated sample is assigned to a solid-state cluster **1** as Figs. 9 and 10 show, its experimental formula is $Mo_6Cl_{11.4}$ on average. The total percentage of Mo (57.6%) and Cl (40.5%) in the 400 °C-treated sample is 98.1%, and hence the rest amounts to 1.9%.

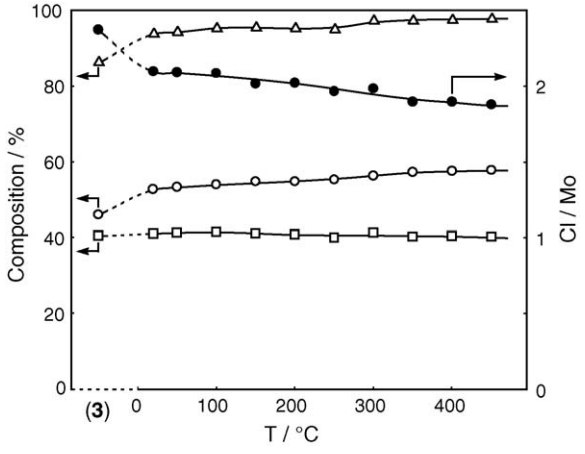

Fig. 12. Analytical data of $(H_3O)_2[(Mo_6Cl_8)Cl_6]\cdot 6H_2O$ (**3**) treated at various temperatures in a helium stream (2.4 L/h) for 1 h. Analytical data for intact **3** are also plotted. Mo (◯), Cl (□), the sum of Mo and Cl (△), and the atomic number ratio of Cl/Mo (●).

Some components presumably originating from the water contained in **3** were left in the treated sample. The formation of hydroxo clusters such as $[(Mo_6Cl_8)Cl_3(OH)(H_2O)_2]$ [61] and $[(Mo_6Cl_8)Cl_2(OH)_2(H_2O)_2]$ [62] have been reported by hydrolysis of **1** in aqueous solutions. Assuming that the rest is composed of the hydroxyl group, the experimental formula of the 400 °C-treated sample is $[(Mo_6Cl_8)Cl_{3.4}(OH)_{1.1}]$.

Intense evolution of HCl was detected when **3** was treated at ambient temperature and above 200 °C. The evolution of HCl by treatment at ambient temperature is explained by Eq. (3); however, no HCl is released during the conversion of **4** to **5** and **1**, as Eqs. (4) and (5) show. Nevertheless, the evolution of HCl was detected above 300 °C. By taking account of these findings and the electronegativity of molybdenum, we deduced that the apical halogen ligand of **5** partially reacted with the aqua ligand eliminating HCl to afford hydroxo complex such as $[(Mo_6Cl_8)Cl_3(OH)(H_2O)]$, when the cluster was treated above 200 °C as expressed by Eq. (6).

$$[(Mo_6Cl_8)Cl_4(H_2O)_2](\mathbf{5}) \xrightarrow{>200\,^\circ C} [(Mo_6Cl_8)Cl_3(OH)(H_2O)] + HCl \quad (6)$$

The hydroxo cluster $[(Mo_6Cl_8)Cl_2(OH)_2(H_2O)_2]$ has been reported as a weak acid to afford protons in aqueous solution [62], and the IR analyses of adsorbed pyridine on $(H_3O)_2[(W_6Cl_8)Cl_6]\cdot 6H_2O$ treated at 450 °C showed the presence of a Brønsted acid site, but no Lewis acid site [22]. The decomposition of phenyl acetate is generally catalyzed by a Brønsted acid site, as mentioned above. Hence, the catalytic activity of the cluster can be attributed to a Brønsted acidity originating from the hydroxo ligand, as exemplified by Eq. (7). The negligible catalytic activity of Re_3Cl_9 shown in Table 1 is in conformity with this conclusion.

$$[(Mo_6Cl_8)Cl_3(OH)(H_2O)] \rightarrow H^+ + [(Mo_6Cl_8)Cl_3(O)(H_2O)]^- \quad (7)$$

On the other hand, the catalytically active sample that had been treated above 250 °C is not a molecular cluster, but the solid-state cluster **1**, as proved by XRD and Raman analyses. This disagreement can be interpreted in terms of the formation of an imperfect crystal including the defective $\{[Mo_6Cl_8^i]Cl_2^aCl_{4/2}^{a-a}\}$ moiety. That is to say, the catalytically active cluster moiety that has a hydroxo ligand such as $\{[Mo_6Cl_8^i]Cl_2^aCl_{3/2}^{a-a}(OH)\}$ or $\{[Mo_6Cl_8^i]Cl^aCl_{4/2}^{a-a}(OH)\}$ was retained intact in the imperfect crystal lattice of the solid-state cluster **1**, as illustrated in Fig. 13, until decay of the cluster initiates above 400 °C. In contrast, catalytically active analogous hydroxo moieties of the Nb cluster such as $[(Nb_6Cl_{12})Cl(OH)(H_2O)_3]$ formed from **2** commenced to decay above 300 °C, because **2** cannot be changed to the corresponding solid-state cluster by heating.

Thus, when **3** was subjected to progressively higher temperatures in a helium stream, **3** changed via **4** to **5** as a solid-phase reaction up to 150 °C. None of these clusters had a catalytic activity. When the temperature increased above 200 °C, cluster **5** changed to Cl-deficient solid-state cluster **1** containing hydroxo

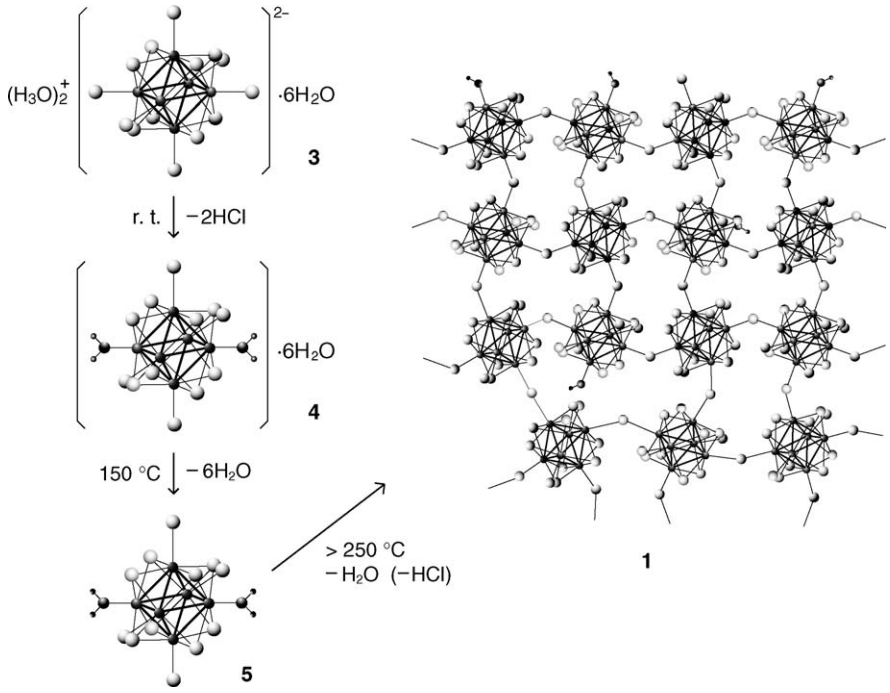

Fig. 13. Conversion of $(H_3O)_2[(Mo_6Cl_8)Cl_6]\cdot 6H_2O$ (**3**) via $[(Mo_6Cl_8)Cl_4(H_2O)_2]\cdot 6H_2O$ (**4**) and $[(Mo_6Cl_8)Cl_4(H_2O)_2]$ (**5**) to the solid-state cluster $[Mo_6Cl_8^i]Cl_2^aCl_{4/2}^{a-a}$ (**1**) containing Brønsted acid sites and crystal defects.

ligand with retention of the cluster framework, which was catalytically active. Then, the activity waned for treatment above 400 °C, at which temperature the decomposition of the cluster commenced to produce amorphous compounds.

3.4. Reaction mechanism

The radical cation of phenyl acetate decomposes through a unimolecular four-centered transition state affording phenol radical cation and ketene [63,64]. The thermal decomposition of phenyl acetate proceeds above ca. 700 °C [35] by way of a similar four-centered cyclic transition state yielding phenol and ketene [36]. This mechanism, a 1,3-H shift of the CH_3CO group of phenyl acetate with simultaneous cleavage of the C–O bond, is ascertained by calculation of the energy profile [65]. The cluster catalysts yielded phenol and ketene exclusively, as in the case of the thermal decomposition. Nevertheless, the cluster catalysis proceeded at as low as 150 °C, implying another reaction mechanism.

The cluster catalysts have a Brønsted acid site, and a mechanism for phenyl acetate transformation over solid Brønsted acids has been proposed [28,31,66]. Phenyl acetate is adsorbed on the protic center and then either rearranges into *o*-hydroxyacetophenone (intramolecular Fries rearrangement) or desorbs as phenol. In the latter case, the residual acetyl cation on the Brønsted base can react with the produced phenol to form *o*- and *p*-hydroxyacetophenone (intermolecular Fries rearrangement), or afford ketene (decomposition) regenerating the Brønsted acid site, as shown in Fig. 14. The stability of the adsorbed species would determine the selectivity for the products.

Ring-attachment isomerization of diethylbenzenes over CF_3COOH [67], Al_2O_3-HCl [68], and Y-zeolite [69] is always accompanied by the formation of the disproportionation products, ethylbenzene and 1,2,4-triethylbenzene, indicating that the intermolecular mechanism is by way of an ethyl cation, which would be stabilized by the counter anion or the conjugate base. On the other hand, cluster catalysts do not yield such by-products in this reaction, demonstrating an intramolecular mechanism without yielding the ethyl cation as an intermediate [21]. Solid acid–base catalysts such as Al_2O_3 and SiO_2-Al_2O_3 nonselectively catalyze transalkylation, dehydrogenation, condensation, and deamination of diethylamine [70–72]. The ethyl group would be eliminated as an ethyl cation by the catalysts. In contrast, halide clusters catalyze dehydrogenation selectively to yield *N*-ethylideneethylamine [23], and the same selectivity is observed over 12-molybdophosphoric acid [73], which is characterized by very weak basicity, great softness, and a large polyhedral anion structure [74–76]. The cluster anions are also large, and hence have very low charge densities on their surface (Eq. (7)). The anion would not participate in the reactions nor stabilize the counter cation. Protonated phenyl acetate and acetyl cation would rapidly disproportionate successively into phenol, ketene, and proton. Consequently, a high-performance catalyst for the Fries rearrangement is expected to have a stabilizing capacity for the cations. Increasing selectivity for the Fries rearrangement [26,27] as well as increasing *p*/*o* ratio of hydroxyacetophenone [77] with decreasing reaction temperature agrees with this interpretation. Liquid phase reaction exhibited better selectivity for the Fries rearrangement compared with the gas phase reaction [27], in which no solvation for the cations is present.

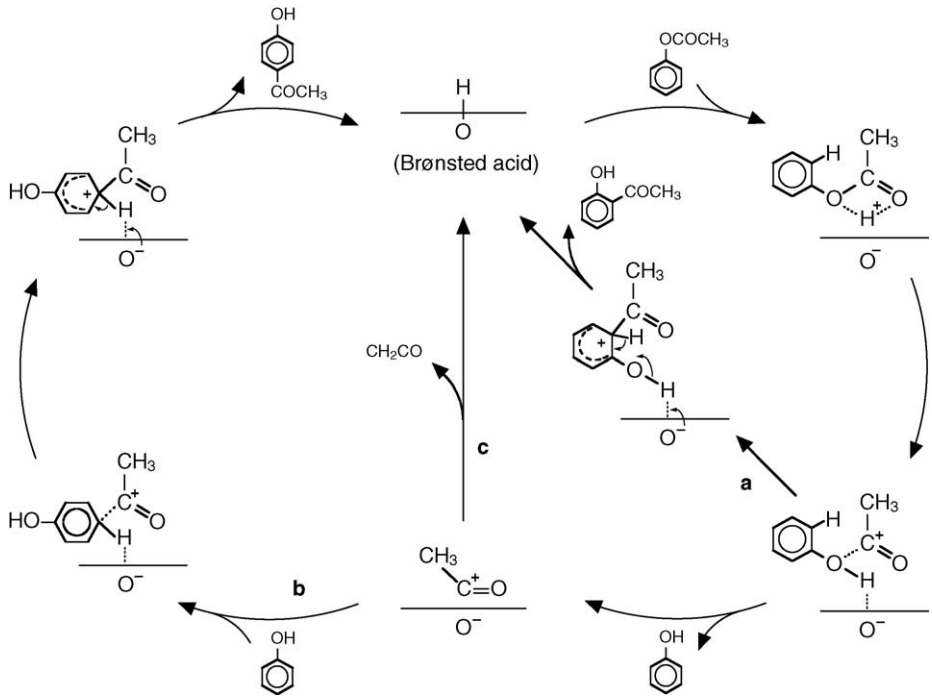

Fig. 14. Reaction mechanism of phenyl acetate over a Brønsted acid site. (a) Intramolecular Fries rearrangement, (b) intermolecular Fries rearrangement, and (c) decomposition.

Oxide catalysts generally have both acidic and basic characters. Alumina has been classified as a solid acid; however, it has both acidic and basic sites: incompletely coordinated aluminum ions (strong Lewis acids) and oxide ions (weak Lewis bases) [78–81]. Both of the sites are small and have high charge densities for participation in reactions. Over conventional solid Brønsted acids such as H-Beta, H-Y, H-ZSM-5, and HF/Al_2O_3, the Fries rearrangement proceeds to some extent, as mentioned above. These catalysts have both acidic and basic sites, in contrast to the cluster catalysts. When Nafion-H catalyst was diluted with SiO_2 to 40 wt.% and 13 wt.%, the selectivity for *o*- and *p*-hydroxyacetophenone increased from 19% to 41% and 50%, respectively [34]. The protonated species would be stabilized by the weak Lewis basic site of SiO_2. Moreover, the *p*/*o* ratio, which is an index of intermolecular reaction, increased from 1.4 to 1.9 and 2.3 demonstrating increased longevity of the acetyl cation by dilution with SiO_2.

4. Conclusions

The molecular halide clusters of Nb, Mo, Ta, and W are stable complexes and had no catalytic activity. However, treatment at 250 °C in a helium stream produced catalytic activity for the selective decomposition of phenyl acetate to phenol and ketene. When Nb cluster **2** was heated under helium, the crystal structure decayed at 100 °C. The molecular structure commenced to change at around 200 °C by losing the outer Cl ligands to develop catalytic activity. At 250 °C small amounts of the internal Cl ligands were removed leaving the Nb_6 cluster framework intact, at which temperature the catalytic activity was a maximum. Above 300 °C the catalytic activity decreased and the cluster framework began to decay. In the case of Mo cluster **3**, it changed to molecular cluster **5** via **4** when the temperature was raised to 150 °C. These clusters had no catalytic activity. The initiation temperature for activity, 200–250 °C, was the degradation temperature for molecular cluster **5** to solid-state cluster **1** of low crystallinity. The most active species that was produced by 400 °C treatment retained the Mo_6 octahedral structure. Above this temperature the cluster framework initiated degradation. In the case of the Mo cluster, the active species was kept in the network of the solid-state cluster, and hence the activity was maintained to higher temperatures than that for the Nb cluster. The activity of the cluster catalyst is ascribed to the Brønsted acidity of the hydroxo ligand that is produced by elimination of hydrogen halide from the halogen and the aqua ligands. Exclusive formation of phenol and ketene is attributable to rapid decomposition of the protonated phenyl acetate and successive decomposition of the acetyl cation, which are not stabilized by the large cluster counter anion.

References

[1] J.D. Corbett, Pure Appl. Chem. 64 (1992) 1359.
[2] J.D. Corbett, NATO ASI ser., Ser. C, Math. Phys. Sci 382 (1992) 27.
[3] S.C. Lee, R.H. Holm, Angew. Chem. Int. Ed. Engl. 29 (1990) 840.
[4] D.M.P. Mingos, D.J. Wales, Introduction to Cluster Chemistry, Prentice-Hall, New Jersey, 1990.
[5] A.W. Struss, J.D. Corbett, Inorg. Chem. 17 (1978) 965.
[6] H. Imoto, J.D. Corbett, A. Cisar, Inorg. Chem. 20 (1981) 145.
[7] I. Nowak, M. Ziolek, Chem. Rev. 99 (1999) 3603.
[8] N. Prokopuk, D.F. Shriver, Adv. Inorg. Chem. 46 (1999) 1.
[9] G.J. Miller, J. Alloys Compd. 229 (1995) 93.
[10] W. Blomstrand, J. Prakt. Chem. 77 (1859) 88.

[11] H. Schäfer, H.G. Schnering, J. Tillack, F. Kuhnen, H. Wöhrle, H. Baumann, Z. Anorg. Allg. Chem. 353 (1967) 281.
[12] H.G. Schnering, W. May, K. Peters, Z. Kristallogr. 208 (1993) 38.
[13] H. Schäfer, H.G. Schnering, Angew. Chem. 76 (1964) 833.
[14] L. Brewer, L.A. Bromley, P.W. Gilles, N.L. Lofgren, Natl. Nucl. Energy Ser. Div. IV B 19 (1950) 276.
[15] H. Schäfer, H.-G. Schnering, J. Tillack, F. Kuhnen, H. Wöhrle, H.Z. Baumann, Anorg. Allgem. Chem. 353 (1967) 281.
[16] S. Kamiguchi, S. Iketani, M. Kodomari, T. Chihara, J. Cluster Sci. 15 (2004) 19.
[17] S. Kamiguchi, S. Nishida, M. Kodomari, T. Chihara, J. Cluster Sci. 16 (2005) 77.
[18] S. Kamiguchi, T. Chihara, Catal. Lett. 85 (2003) 97.
[19] S. Kamiguchi, M. Noda, Y. Miyagishi, S. Nishida, M. Kodomari, T. Chihara, J. Mol. Catal. A 195 (2003) 159.
[20] S. Kamiguchi, M. Watanabe, K. Kondo, M. Kodomari, T. Chihara, J. Mol. Catal. A 203 (2003) 153.
[21] S. Kamiguchi, K. Kondo, M. Kodomari, T. Chihara, J. Catal. 223 (2004) 54.
[22] S. Kamiguchi, S. Nishida, H. Kurokawa, H. Miura, T. Chihara, J. Mol. Catal. A 226 (2005) 1.
[23] S. Kamiguchi, A. Nakamura, A. Suzuki, M. Kodomari, M. Nomura, Y. Iwasawa, T. Chihara, J. Catal. 230 (2005) 204.
[24] A.H. Blatt, Org. React. 1 (1942) 342.
[25] H. Koningsveld, J.J. Scheele, J.C. Jansen, Acta Cryst. C43 (1987) 294.
[26] A.H.G. Vogt, H.W. Kouwenhoven, Collect. Czech. Chem. Commun. 57 (1992) 853.
[27] A. Vogt, H.W. Kouwenhoven, R. Prins, Appl. Catal. A 123 (1995) 37.
[28] U. Freese, F. Heinrich, F. Roessner, Catal. Today 49 (1999) 237.
[29] H. Bekkum, A.J. Hoefnagel, M.A. Koten, E.A. Gunnewegh, A.H.G. Vogt, H.W. Kouwenhoven, Stud. Surf. Sci. Catal. 83 (1994) 379.
[30] Y. Pouilloux, N.S. Gnep, P. Magnoux, G. Perot, J. Mol. Catal. 40 (1987) 231.
[31] Y. Pouilloux, J.-P. Bodibo, I. Neves, M. Gubelmann, G. Perot, M. Guisnet, Stud. Surf. Sci. Catal. 59 (1991) 513.
[32] C.S. Cundy, R. Higgins, S.A.M. Kibby, B.M. Lowe, R.M. Paton, Tetrahedron Lett. 30 (1989) 2281.
[33] V. Borzatta, G. Busca, E. Poluzzi, V. Rossetti, M. Trombetta, A. Vaccari, Appl. Catal. A 257 (2004) 85.
[34] A. Heidekum, M.A. Harmer, W.F. Hoelderich, J. Catal. 176 (1998) 260.
[35] E. Ghibaudi, A.J. Colussi, Int. J. Chem. Kinet. 16 (1984) 1575.
[36] E. Ghibaudi, A.J. Colussi, J. Chem Soc., Chem. Commun. (1984) 433.
[37] T. Chihara, S. Kamiguchi, Chem. Lett. (2002) 70.
[38] F.W. Koknat, J.A. Parsons, A. Vongvusharintra, Inorg. Chem. 13 (1974) 1699.
[39] P. Nannelli, B.P. Block, Inorg. Synth. 12 (1970) 170.
[40] V. Kolesnichenko, L. Messerle, Inorg. Chem. 37 (1998) 3660.
[41] E.A. Stern, M. Newville, B. Ravel, Y. Yacoby, D. Haskel, Physica B 208 (1995) 117.
[42] M. Newville, P. Livins, Y. Yacoby, E.A. Stern, J.J. Rehr, Phys. Rev. B 47 (1993) 14126.
[43] A.L. Ankudinov, B. Ravel, J.J. Rehr, S.D. Conradson, Phys. Rev. B 58 (1998) 7565.
[44] A. Simon, H.G. Schnering, H. Wöhrle, H. Schäfer, Z. Anorg. Allg. Chem. 339 (1965) 155.
[45] P.M. Boorman, B.P. Straughan, J. Chem. Soc. A (1966) 1514.
[46] K. Harder, W. Preetz, Z. Anorg. Allg. Chem. 591 (1990) 32.
[47] J.R. Schoonover, T.C. Zietlow, D.L. Clark, J.A. Heppert, M.H. Chisholm, H.B. Gray, A.P. Sattelberger, W.H. Woodruff, Inorg. Chem. 35 (1996) 6606.
[48] N. Brnicevic, B. Kojic-Prodic, M. Luic, A. Kashta, P. Planinic, R.E. McCarley, Croat. Chem. Acta 68 (1995) 861.
[49] E.P. Parry, J. Catal. 2 (1963) 371.
[50] A. Fratiello, J.P. Luongo, J. Am. Chem. Soc. 85 (1963) 3072.
[51] D. Cook, Can. J. Chem. 39 (1961) 2009.
[52] C. Brosset, Arkiv Kemi Mineral. Geol. A 22 (11) (1964) 1.
[53] L.J. Guggenberger, A.W. Sleight, Inorg. Chem. 8 (1969) 2041.
[54] H. Schäfer, H. Plautz, Z. Anorg. Allg. Chem. 389 (1972) 57.
[55] A. Zelverte, S. Mancour, P. Caillet, Spectrochim. Acta A 42 (1986) 837.
[56] D. Hartley, M.J. Ware, J. Chem. Soc., Chem. Commun. (1967) 912.
[57] S. Senderoff, A. Brenner, J. Electrochem. Soc. 101 (1954) 16.
[58] Y. Saeki, R. Matsuzaki, T. Matsushima, Denki Kagaku 35 (1967) 298.
[59] R. Matsuzaki, Y. Saeki, J. Less-Common Met. 29 (1972) 427.
[60] R. Matsuzaki, Y. Saeki, Denki Kagaku 35 (1967) 448.
[61] J.C. Sheldon, J. Chem. Soc. (1960) 1007.
[62] C. Brosset, Arkiv. Kemi. 1 (1950) 353.
[63] D.J. Underwood, J.H. Bowie, J. Chem. Soc., Perkin Trans. 2 (1977) 1670.
[64] S.A. Benezra, M.M. Bursey, J. Chem. Soc. B (1971) 1515.
[65] I. Lee, C.K. Kim, B.-S. Lee, J. Chem. Res. (S) (1990) 42.
[66] I. Neves, F. Jayat, P. Magnoux, G. Pérot, F.R. Ribeiro, M. Gubelmann, M. Guisnet, J. Mol. Catal. 93 (1994) 169.
[67] H.J. Bakoss, R.M.G. Roberts, A.R. Sadri, J. Org. Chem. 47 (1982) 4053.
[68] N. Nambu, K. Yamamoto, S. Hamanaka, M. Ogawa, Nippon Kagaku Kaishi (1979) 925.
[69] A.P. Bolton, M.A. Lanewala, P.E. Pickert, J. Org. Chem. 33 (1968) 1513.
[70] B.Q. Xu, T. Yamaguchi, K. Tanabe, Appl. Catal. 75 (1991) 75.
[71] J. Sedlacek, J. Koubek, Collect. Czech. Chem. Commun. 48 (1983) 755.
[72] M.F. Ebeid, J. Pasek, Collect. Czech. Chem. Commun. 35 (1970) 2166.
[73] A.-G.A. Ali, L.I. Ali, Collect. Czech. Chem. Commun. 60 (1995) 2047.
[74] Y. Izumi, K. Matsuo, K. Urabe, J. Mol. Catal. 18 (1983) 299.
[75] T. Okuhara, N. Mizuno, M. Misono, Adv. Catal. 41 (1996) 113.
[76] N. Mizuno, M. Misono, Chem. Rev. 98 (1998) 199.
[77] P.B. Venuto, P.S. Landis, Adv. Catal. 18 (1968) 259.
[78] J.B. Peri, J. Phys. Chem. 69 (1965) 220.
[79] J. Koubek, J. Volf, J. Pasek, J. Catal. 38 (1975) 385.
[80] P. Hogan, J. Pasek, Collect. Czech. Chem. Commun. 38 (1973) 1513.
[81] S. Rajagopal, T.L. Grimm, D.J. Collins, R. Miranda, J. Catal. 137 (1992) 453.